

Original Article



Induction of Anti-Aquaporin 5 Autoantibody Production by Immunization with a Peptide Derived from the Aquaporin of *Prevotella melaninogenica* Leads to Reduced Salivary Flow in Mice

OPEN ACCESS

Received: Jun 18, 2021
Revised: Sep 19, 2021
Accepted: Oct 14, 2021

*Correspondence to
Junho Chung

Department of Biochemistry and Molecular Biology, Seoul National University College of Medicine, 101 Daehak-ro, Jongno-gu, Seoul 03080, Korea.
E-mail: jhchung@snu.ac.kr

Youngnim Choi

Department of Immunology and Molecular Microbiology, School of Dentistry and Dental Research Institute, Seoul National University, 101 Daehak-ro, Jongno-gu, Seoul 03080, Korea.
E-mail: youngnim@snu.ac.kr

*Ahreum Lee, Duck Kyun Yoo, and Yonghee Lee contributed equally.

Copyright © 2021. The Korean Association of Immunologists

This is an Open Access article distributed under the terms of the Creative Commons Attribution Non-Commercial License (<https://creativecommons.org/licenses/by-nc/4.0/>) which permits unrestricted non-commercial use, distribution, and reproduction in any medium, provided the original work is properly cited.

ORCID iDs

Duck Kyun Yoo <https://orcid.org/0000-0002-3341-4897>
Yonghee Lee <https://orcid.org/0000-0001-8095-408X>
Suhan Jung <https://orcid.org/0000-0002-4301-9065>
Jinsung Noh <https://orcid.org/0000-0002-7167-8113>

Ahreum Lee^{1,†}, Duck Kyun Yoo ^{2,3,†}, Yonghee Lee ^{4,†}, Sumin Jeon¹,
Suhan Jung ⁵, Jinsung Noh ⁴, Soyeon Ju ^{2,3}, Siwon Hwang ^{2,3},
Hong Hee Kim⁵, Sunghoon Kwon^{4,6,7,8,9}, Junho Chung ^{1,*}, Youngnim Choi ^{1,*}

¹Department of Immunology and Molecular Microbiology, School of Dentistry and Dental Research Institute, Seoul National University, Seoul 03080, Korea

²Department of Biochemistry and Molecular Biology, Seoul National University College of Medicine, Seoul 03080, Korea

³Department of Biomedical Science, Seoul National University College of Medicine, Seoul 03080, Korea

⁴Department of Electrical and Computer Engineering, Seoul National University, Seoul 08826, Korea

⁵Department of Cell and Developmental Biology, School of Dentistry and Dental Research Institute, Seoul National University, Seoul 08826, Korea

⁶Interdisciplinary Program in Bioengineering, Seoul National University, Seoul 08826, Korea

⁷BK21+ Creative Research Engineer Development for IT, Seoul National University, Seoul 08826, Korea

⁸Biomedical Research Institute, Seoul National University Hospital, Seoul 03080, Korea

⁹Institutes of Entrepreneurial BioConvergence, Seoul National University, Seoul 08826, Korea


¹⁰Cancer Research Institute, Seoul National University College of Medicine, Seoul 03080, Korea

ABSTRACT

Sjögren's syndrome (SS) is an autoimmune disease characterized by dryness of the mouth and eyes. The glandular dysfunction in SS involves not only T cell-mediated destruction of the glands but also autoantibodies against the type 3 muscarinic acetylcholine receptor or aquaporin 5 (AQP5) that interfere with the secretion process. Studies on the breakage of tolerance and induction of autoantibodies to these autoantigens could benefit SS patients. To break tolerance, we utilized a PmE-L peptide derived from the AQP5-homologous aquaporin of *Prevotella melaninogenica* (PmAqp) that contained both a B cell “E” epitope and a T cell epitope. Repeated subcutaneous immunization of C57BL/6 mice with the PmE-L peptide efficiently induced the production of Abs against the “E” epitope of mouse/human AQP5 (AQP5E), and we aimed to characterize the antigen specificity, the sequences of AQP5E-specific B cell receptors, and salivary gland phenotypes of these mice. Sera containing anti-AQP5E IgG not only stained mouse Aqp5 expressed in the submandibular glands but also detected PmAqp and PmE-L by immunoblotting, suggesting molecular mimicry. Characterization of the AQP5E-specific autoantibodies selected from the screening of phage display Ab libraries and mapping of the B cell receptor repertoires revealed that the AQP5E-specific B cells acquired the ability to bind to the Ag through cumulative somatic hypermutation. Importantly, animals with anti-AQP5E Abs had decreased salivary flow rates without immune cell infiltration into the salivary glands. This model will be useful for

Soyeon Ju 

<https://orcid.org/0000-0002-9798-8785>

Siwon Hwang 

<https://orcid.org/0000-0002-7546-2491>

Junho Chung 

<https://orcid.org/0000-0002-3436-9389>

Youngnim Choi 

<https://orcid.org/0000-0002-6496-5560>

Conflict of Interest

The authors declare no potential conflicts of interest.

Abbreviations

APC, Ag presenting cell; AQP5, aquaporin 5; AQP5E, "E" epitope of mouse/human AQP5; BCR, B cell receptor; CDR, complementarity determining region; IFA, incomplete Freund's adjuvant; M3R: type 3 muscarinic acetylcholine receptor; NGS, next-generation sequencing; OD, optical density; Pm, *Prevotella melaninogenica*; PmAqp, aquaporin of *Prevotella melaninogenica*; SHM, somatic hypermutation; SS, Sjögren's syndrome; SSA, SS-related Ag A; SSB, SS-related Ag B.

Author Contributions

Conceptualization: Chung J, Choi Y; Methodology: Jung S, Noh J; Investigation: Lee A, Yoo DK, Lee Y, Jeon S, Ju S, Hwang S; Validation: Jung S, Chung J, Kwon S, Kim HH; Formal analysis: Lee A, Yoo DK, Lee Y; Funding acquisition: Choi Y; Data curation: Lee A, Yoo DK, Lee Y; Original draft preparation: Lee A, Yoo DK, Lee Y; Review and editing: Jeon S, Jung S, Noh J, Ju S, Hwang S, Kim HH, Kwon S, Chung J, Choi Y.

investigating the role of anti-AQP5 autoantibodies in glandular dysfunction in SS and testing new therapeutics targeting autoantibody production.

Keywords: Sjogren's syndrome; Autoantibodies; Aquaporin-5; Molecular mimicry; Mice

INTRODUCTION

Sjögren's syndrome (SS) is an autoimmune disease characterized by dry mouth, dry eyes, and focal lymphocytic infiltration of the salivary/lacrimal glands (1,2). Hypergammaglobulinemia and the production of various autoantibodies, including those against SS-related Ag A (SSA), SS-related Ag B (SSB), IgG, type 3 muscarinic acetylcholine receptor (M3R), and aquaporin 5 (AQP5), are also features of SS (3-5). The glandular dysfunction in SS involves not only the destruction of acinar cells by infiltrated T cells but also the presence of autoantibodies against M3R or AQP5 that interfere with the secretion process. AQP5 is a major water channel protein expressed in the lacrimal and salivary glands and plays a critical role in tear and saliva secretion (6). Three functional epitopes for the anti-AQP5 autoantibodies have been mapped at extracellular loops A, C, and E of AQP5 (7). The presence of anti-AQP5 autoantibodies was associated with low salivary flow rates in patients from the Korean Initiative of Primary Sjogren's Syndrome but not in those from the Sjögren's International Collaborative Clinical Alliance registry (5,8).

The production of autoantibodies is the result of breached self-tolerance. B cells acquire tolerance to self-Ags during development in the bone marrow and maturation in peripheral lymphoid tissues via deletion, receptor editing, or anergy (9-11). Infection is a common environmental factor associated with autoimmune diseases and is thought to disrupt self-tolerance through bystander activation of Ag-presenting cells (APCs) or molecular mimicry. APCs activated by microbes can result in the activation of self-reactive T cells. In molecular mimicry, B cells or T cells activated by microbial Ags cross-react with autoantigens that have the sequence or conformational homologies with the microbial Ags.

The salivary glands, one of the target organs of SS, are inevitably affected by bacteria colonizing the oral cavity, and several studies have reported an altered oral microbiota in SS (12-14). Ductal cells and the areas of lymphocytic infiltration in the labial salivary glands from patients with SS are heavily infected with bacteria, including the oral commensal *Prevotella melaninogenica* (Pm). The aquaporin of Pm (PmAqp) is highly homologous to human AQP5, particularly at the regions of extracellular loop E and intracellular loop B that form a single narrow aqueous pathway (15-17).

Recently, we investigated whether PmAqp-derived peptides, namely, the linear and cyclic forms of PmE-L that contain both a B cell "E" epitope and a T cell epitope, can induce the production of anti-AQP5 autoantibodies and reported that immunization with the cyclized form of PmE-L induced the production of autoantibodies against the "E" epitope of mouse/human AQP5 (AQP5E) along with Abs against PmE, a Pm homolog of AQP5E, in 100% of the C57BL/6 immunized mice (17). However, whether this model displays the features of SS is unclear. In this study, we characterized an anti-AQP5 autoantibody-producing mouse model by investigating Ag specificity, salivary gland phenotypes, and the sequences of AQP5E-specific B cell receptors.

MATERIALS AND METHODS

3D structure modeling

The structures of mouse Aqp5 (accession: NP_033831.1) and PmAqp (accession: BBA28519.1) were constructed on the SWISS_MODEL server (<https://swissmodel.expasy.org/>) using a known human AQP5 structure (structure ID: PDB 3D9S) as a template. The 3D structures of peptides used for either immunization or ELISA were predicted at the PEP-FOLD3 server (<https://mobyle.rpbs.univ-paris-diderot.fr/cgi-bin/portal.py#forms::PEP-FOLD3/>).

Mice

The experimental protocols and animal handling procedures were approved by the Seoul National University Animal Care and Use Committee, Seoul, Republic of Korea (No. SNU-180508-2-2). Female C57BL/6 mice purchased from Orient Bio (Seongnam, Korea) were maintained under specific pathogen-free conditions in the laboratory animal facility at the School of Dentistry, Seoul National University. Mice used in experiments were 6-wk old.

Bacterial lysates and peptides

Pm KCTC 5457 (Korean Collection for Type Cultures, Daejeon, Korea) was anaerobically cultured in modified PYG medium supplemented with 10 µg/ml vitamin K and 5 µg/ml hemin. After washing with PBS, bacteria resuspended in PBS at 1×10^8 cells/ml were lysed by repeated freeze-thaw cycles. Peptides used for immunization and ELISA were synthesized by Pepton (Daejeon, Korea). The sequences of peptides are previously reported (17). The M3R Ag peptide (biotin-SCIPKTYWNC [C-C]) for ELISA was slightly modified from the previously reported one by adding biotin and serine to the N-terminus (18).

Immunization

To induce anti-AQP5 autoantibodies, mice were primed with 100 µl of Pm lysate on day 0 and boosted with either 100 µl of Pm lysate or 100 µg of peptide PmE-L (a cyclic form) emulsified in incomplete Freund's adjuvant (IFA) on days 10, 24, and 38. As controls, mice in the sham group received PBS and IFA alone for priming and boosting, respectively. All immunizations were performed by subcutaneous injection on both sides of the tail base. Mice were sacrificed 10–14 days after the last boosting.

Measurement of salivary flow rate

After anesthesia, pilocarpine (5 mg/kg of body weight) was intraperitoneally administered to stimulate saliva secretion. Saliva was collected for 10 min after pilocarpine stimulation and weighed. The salivary flow rate was expressed as mg of saliva/g of body weight.

Flow cytometry

Single-cell suspensions of the draining (inguinal) lymph nodes of immunized mice were prepared. Cells were stained with FITC-conjugated AQP5E peptide (Pepton), anti-CD19 (PE-Cy7-6D5 from BioLegend, San Diego, CA, USA), anti-GL7 (eFluor 660-GL7 from eBioscience, San Diego, CA, USA), anti-CD38 (BV605-90 from BD Bioscience, Franklin Lakes, NJ, USA), and Ghost Dye™ viability dye (Tonbo, San Diego, CA, USA). The data were acquired on an Aria II flow cytometer (BD Bioscience) and analyzed using FlowJo software after gating live cells based on the forward scatter and exclusion of Ghost Dye™.

Histology and indirect immunofluorescence

The submandibular salivary glands from mice were fixed in 4% paraformaldehyde at 4°C, cryopreserved with 10% to 30% sucrose, and embedded in OCT compound (Sakura Finetek, Torrance, CA, USA). The frozen sections were stained with H&E and examined for focal lymphocytic sialadenitis.

Sections of the salivary glands from the sham group were also used for indirect immunofluorescence. After Ag retrieval by incubation in sodium citrate buffer (10 mM sodium citrate, 0.05% Tween 20, pH=6) at 105°C for 20 min, the sections were blocked with 5% BSA plus goat serum and then incubated with rabbit anti-AQP5 polyclonal Abs (1:100; ATLAS Antibodies, Bromma, Sweden) and mouse sera (1:10) overnight. After washing, the sections were incubated with Alexa Fluor 488–conjugated donkey anti-rabbit IgG (Invitrogen, Carlsbad, CA, USA) and Alexa Fluor 594–conjugated goat anti-mouse IgG (Invitrogen) for 1.5 h. The sections were washed, mounted, and examined by confocal microscopy (Carl Zeiss, Oberkochen, Germany).

ELISA

The levels of anti-SSA (Ro-52) autoantibodies in sera were measured using a kit from Signosis (Santa Clara, CA, USA) according to the manufacturer's instructions.

The levels of anti-PmE-L, anti-PmE, anti-AQP5E, and anti-M3R Abs were determined using biotinylated peptides as Ags. Microplates were coated with 1 µg/well avidin (Sigma, St. Louis, MO, USA) in PBS overnight at 4°C. After blocking with 1% BSA, the plates were incubated with 0.2 µg/well biotinylated Ag peptides in PBS for 1 h at room temperature. After the plates were washed, they were incubated with serum (1:300 dilution) for 1 h at room temperature. In parallel, samples were also incubated in wells coated with avidin alone. After washing, the plates were incubated with HRP-conjugated goat anti-mouse IgG (Southern Biotech, Birmingham, AL, USA) for 1 h at room temperature. The plates were washed on a shaker for 5 min 3 times. Bound HRP-conjugated detection Abs were developed with 3,3',5,5'-tetramethylbenzidine substrate (Sigma). After stopping the enzyme activity by the addition of 2 N H₂SO₄, the optical density (OD) values were measured at 450 nm. To generate a standard curve, serially diluted mouse IgG1 (40 to 0.625 ng/ml, BD Bioscience) was coated in the two columns of each plate instead of Ags. The amount of bound Ag-specific IgG was determined using an equation generated from the standard curve and OD after subtracting that obtained from incubation with avidin alone. The levels of total IgG were determined using a mouse IgG total quantification kit (Invitrogen) according to the manufacturer's instructions.

To determine the Ag-specific binding of phage clones or recombinant IgG, ELISA was performed as described above by incubating the phage clones or recombinant IgG instead of sera. Binding was expressed as the OD.

Immunoblot

Pm lysates (5 and 15 µg) and PmE-L (1 µg) were separated through a 15% SDS-polyacrylamide gel and transferred to a PVDF membrane (Merck Millipore, Billerica, MA, USA) by wet transfer. After blocking with 5% skim milk, the membrane was incubated with sera from immunized mice at a 1:5,000 dilution for 10 h at 4°C. After washing, the membrane was incubated with HRP-conjugated anti-mouse IgG (GenDEPOT, Barker, TX, USA) for 1 h at room temperature. Immunoreactive bands were detected with electrochemiluminescence reagents.

Isolation of AQP5E-specific monoclonal Abs

From the immunized mice, total RNA was isolated from the draining lymph nodes using TRIzol Reagent (Invitrogen), and cDNA was synthesized using the SuperScript IV First-Strand Synthesis System with oligo dT priming (Invitrogen). Using this cDNA, phage-displayed Ab libraries were prepared as described previously (19), and then subjected to seven rounds of biopanning using PmE-conjugated magnetic beads (Invitrogen). After the final round of biopanning, phage clones were subjected to phage ELISA using PmE, AQP5E, and AQP5A peptides as Ags, as described previously with adequate modification (20). The sequences of specific binders that bound to PmE and AQP5E but not to AQP5A were determined by Sanger sequencing (Macrogen, Seoul, Korea).

Next-generation sequencing (NGS)

To analyze the B cell receptor (BCR) repertoire after immunization, double-stranded cDNA libraries were constructed using in-house designed mouse immunoglobulin-specific primers. First-strand cDNA was synthesized using 1 µg total RNA and a SuperScript IV First-Strand Synthesis System and mouse constant gene-specific reverse primers with a P7 sequence (5'-TGACTGGAGTTCAGACGTGTGCTCTTCCGATCT-3') and a UMI barcode (21). Synthesized cDNA was purified using AMPure XP beads (Beckman Coulter, Brea, CA, USA) according to the manufacturer's instructions. Second-strand cDNA was synthesized using KAPA HiFi HotStart DNA polymerase (Kappa Bioscience, Oslo, Norway) and mouse variable gene-specific forward primers with a P5 sequence (5'-ACACTCTTCCCTACACGACGCTCTTCCGATCT-3') (98°C for 4 min, 60°C for 1 min, 72°C for 5 min). Double-stranded cDNA was purified using AMPure XP beads and subjected to PCR amplification with KAPA HiFi HotStart DNA polymerase using two universal primers containing Illumina adapters and index sequences (95°C for 3 min; 25 cycles of 95°C for 30 s, 65°C for 30 s, and 72°C for 1 min; and 72°C for 5 min). The final products were purified using AMPure XP beads and subjected to a quality control procedure on TapeStation 2200 (Agilent Technologies, Santa Clara, CA, USA) as previously described (20). Libraries with a single peak of the correct sequence length were subjected to NGS analysis using the MiSeq platform (Illumina Inc., San Diego, CA, USA) with 2 × 300 paired-end run mode. All NGS raw data are available at the National Center for Biotechnology Information Sequencing Read Archive (www.ncbi.nlm.nih.gov/sra) under PRJNA739054.

Processing and mapping of the NGS data

All raw paired FASTQ files were subjected to the following processes: i) paired-end merging and quality filtering, ii) error correction, and iii) region annotation. Paired-end merging was performed using PEAR software (22) with default parameters, followed by quality filtering using an in-house Python 3.6 script with the Q20P95 option, which extracted the reads if more than 95% of bases had a Phred quality score > 20. Error correction on quality-filtered data was performed based on the unique molecular identifier, following the previously described methodology (23). In the annotation process, the V/D/J gene, complementarity determining regions (CDRs; CDR1, CDR2, and CDR3), isotype, and divergence from the V gene were obtained using the IgBLAST tool (24) with the Ig germline database of C57BL/6 mice acquired from the IMGT database (25). The divergence from the V gene was defined as the ratio of somatic hypermutations (SHM) in the V gene region.

From the five mice, a total of 680,326 error-corrected reads were obtained, from which a total of 669,459 functional reads were annotated (Table 1). To normalize the data size, 25,800 sequences in each repertoire were randomly sampled, and the sampling size was chosen

Table 1. Sequencing statistics

Sample	Q-filtered	Error corrected	Annotated reads	Functional reads	UMI ratio
M1	1,398,908	60,417	59,802	58,195	4.32
M2	1,894,815	295,614	291,708	295,361	15.6
M3	2,176,279	26,819	26,786	26,330	1.23
M4	2,124,078	26,466	26,384	25,859	1.25
M5	1,809,019	271,010	268,562	263,714	15.0

considering the minimum number of functional sequences among the five repertoires. To identify AQP5E-specific binder-like BCR sequences, dissimilarity to the binder, which was defined as the ratio of Levenshtein distance in the target region (CDR3), was calculated for all unique VDJ sequences in each repertoire.

Production of recombinant IgG specific to AQP5E

The variable genes encoding clone 44 were cloned into a modified expression vector containing the human IgG4 construct, and transfected into Expi293F cells (Invitrogen) as described previously (26). IgG was purified by affinity chromatography using MabSelect columns with the AKTA Pure chromatography system (GE Healthcare, Chicago, IL, USA) following the manufacturer's protocol. An in-house discovered Ab specific to Zika virus envelope domain III (27) was also produced in human IgG4 format and used as an isotype control.

Transepithelial water flow measurement

The osmotic flow of water across a cell monolayer was measured by a previously described method (7). MDCK cells expressing human AQP5 (MDCK-AQP5) were grown on a 0.33-cm² Transwell insert for 4 days until the transepithelial resistances was greater than 320 Ωcm². Recombinant IgG (clone 44) was preabsorbed at 0.5 mg/ml with 1 mg of peptide E or A in serum-free DMEM overnight at 4°C. The cells were incubated with 50 μl of nonabsorbed or preabsorbed IgG on ice for 1 h. After washing, osmotic shock was applied by adding 400 mM D-mannitol to the Transwell insert. After incubation for 20 min at 37°C, the volume of fluid in the Transwell insert was measured. Transepithelial osmotic permeability coefficient P_f^T (μm/s) was calculated as $P_f^T = J_v^T / S v_w \Delta[\Phi]^T$, where J_v^T is the measured transepithelial flow (cm³/s), S is the transwell surface area (0.33 cm²), v_w is the partial molar volume of water (18 cm³/mol), and $\Delta[\Phi]^T$ is the transepithelial osmotic gradient (4×10⁻⁴ mol/cm³) (28).

Statistics

All data obtained from the mouse experiments were analyzed with a nonparametric approach (Kruskal-Wallis or Mann-Whitney test and Spearman's correlation). The difference in the transepithelial osmotic permeabilities was evaluated by Student's t-test.

RESULTS

Compared with mouse Aqp5, PmAqp and peptide Ags had conserved structures at epitope E

PmAqp and the PmE-L peptide that was designed for immunization have two and one amino acid differences, respectively, at the B cell “E” epitope compared with that of mouse Aqp5 (17). The 3D structures of mouse Aqp5, PmAqp, and the Ag peptides used for immunization or ELISAs were predicted, and the 3D structures of the E epitope in mouse Aqp5, PmAqp, and the three peptides were relatively well conserved (Fig. 1).

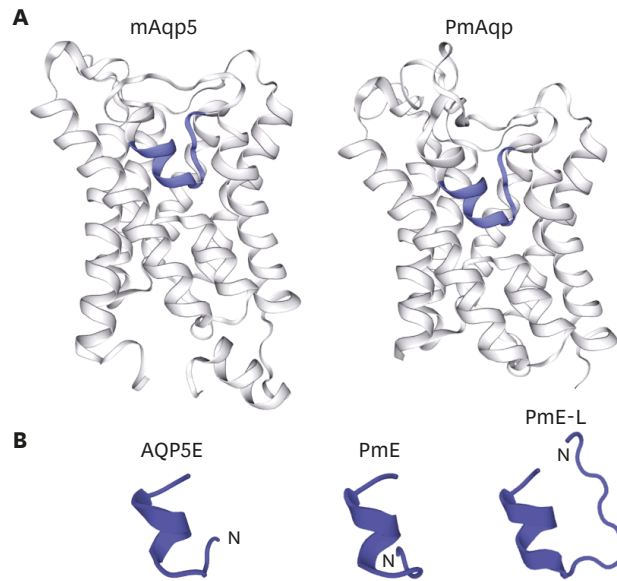


Figure 1. Compared with mouse Aqp5, Pm AQP and peptide Ags had highly conserved structures at epitope E. (A) The structures of the mouse Aqp5 and PmAqp were constructed on the SWISS-MODEL server using the structure of human AQP5 (PDB 3D9S) as a template. Blue highlighting depicts AQP5E and PmE in mouse Aqp5 and PmAqp, respectively. (B) The structures of the peptide Ags were predicted on the PEP-FOLD3 server.

Autoantibodies against AQP5E were induced via molecular mimicry

We previously confirmed that repeated immunization with the PmE-L peptide emulsified in IFA induced autoantibodies against AQP5E. To investigate the possibility that Pm infection induces the production of anti-AQP5 autoantibodies in SS patients, mice were repeatedly immunized with Pm lysate and compared with the mice immunized with PmE-L (**Fig. 2A**). Although the levels of total IgG were increased even more in the Pm group than in the PmE-L group, the levels of IgG Abs against PmE-L, PmE, and AQP5E were significantly increased only in the PmE-L group compared with the sham group. One mouse (11%) in the Pm group produced anti-AQP5E IgG at a concentration above 1 $\mu\text{g/ml}$, a predetermined threshold for Ab positivity, while 8 mice (89%) in the PmE-L group were positive for anti-AQP5E IgG (**Fig. 2B**). A strong positive correlation was observed between the levels of anti-PmE Abs and anti-AQP5E autoantibodies ($r=0.914$, $p<0.0005$; **Fig. 2C**). The frequency of AQP5E-specific germinal center B cells in the draining lymph nodes was examined by flow cytometry using a FITC-conjugated AQP5E peptide (**Fig. 2D**). Expansion of AQP5E-specific cells, along with that of germinal center B cells, was observed in both the Pm and PmE-L groups (**Fig. 2E and F**).

The mice positive for the anti-AQP5E autoantibodies had reduced salivary flow rates (**Fig. 2G**). Although there was a wide variation in the salivary flow rates, the salivary flow rate tended to decrease with increased anti-AQP5E IgG levels (**Fig. 2H**). Despite the reduced salivary flow rate, no pathological changes, including focal lymphocytic sialadenitis, was observed in the salivary glands of the mice (data not shown). Furthermore, anti-SSA autoantibodies were not detected in any of the mice (**Fig. 2I**). Interestingly, anti-M3R autoantibodies were detected in a few mice in each group (**Fig. 2J**).

For confirmation of the antigenic specificity of anti-AQP5E autoantibodies, which was determined by binding to the AQP5E peptide, sections of mouse submandibular salivary glands were double stained with mouse sera and commercial anti-AQP5 Abs. While the anti-AQP5E-positive sera from the PmE-L immunized mice stained Aqp5 in the salivary

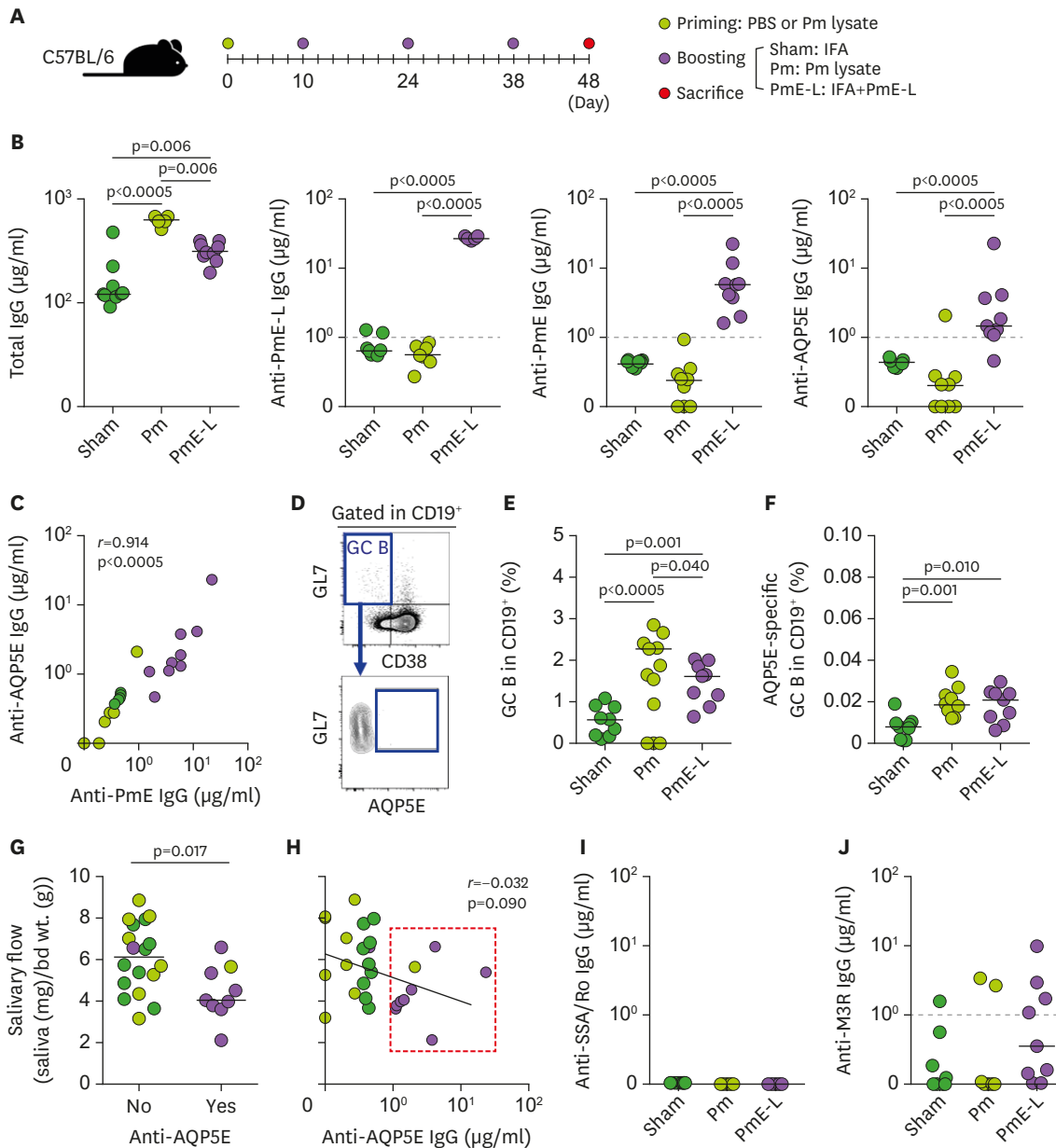


Figure 2. Anti-AQP5 autoantibodies induced were associated with a decreased salivary flow rate. (A) The experimental scheme is shown. (B) The levels of total IgG, anti-PmE, anti-PmE, and anti-AQP5 IgG were determined by ELISAs. Dotted lines indicate the predetermined thresholds for Ab positivity. The horizontal lines present the median of each group. The p-values were determined by the Kruskal-Wallis test followed by post hoc analyses. (C) A correlation plot between the levels of anti-PmE IgG and anti-AQP5 IgG. The p-value was determined by Spearman's correlation method. (D-F) The cells of draining lymph nodes were stained with FITC-conjugated AQP5E peptide and Abs against CD19, CD38, and GL7 and were then analyzed by flow cytometry. A gating strategy for AQP5E-specific germinal center B cells is presented (D). The percentages of germinal center B cells (E) and AQP5E-specific germinal center B cells (F) among CD19⁺ B cells are presented. (G) Salivary flow rates were measured and plotted according to the absence or presence of anti-AQP5 autoantibodies. The p-value was determined by the Mann-Whitney U test. (H) A scatter plot of the levels of anti-AQP5 IgG and salivary flow rates. The red square indicates mice with anti-AQP5 autoantibodies. (I, J) The levels of anti-SSA and anti-M3R IgG were determined by ELISAs.

glands, the sera from the sham group did not (**Fig. 3A**). The binding of Abs produced by immunization with PmE-L to PmAqp was also confirmed by immunoblotting. Multiple bands, including the PmAqp band expected to be 23.6 kDa, were detected by the sera with anti-AQP5 IgG but not by the sera from the sham group (**Fig. 3B**, Lanes 1&2). Antibodies in the immunized sera also detected the PmE-L peptide (**Fig. 3B**, Lane 3). Thus, the foreign Ag PmE-L induced the production of anti-AQP5 autoantibodies via molecular mimicry.

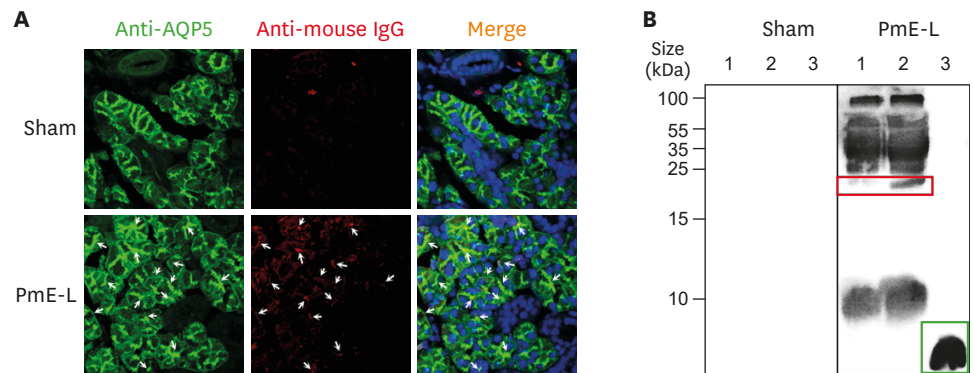


Figure 3. Ag specificity of anti-AQP5E autoantibodies. (A) Sections of the mouse submandibular glands were stained with rabbit anti-Aqp5 Abs and sera from either the sham or PmE-L-immunized mice followed by Alexa Fluor 488-conjugated donkey anti-rabbit IgG and Alexa Fluor 594-conjugated goat anti-mouse IgG. Arrows indicate stained Aqp5. (B) Pm lysates (Lane 1: 5 µg, Lane 2: 15 µg) and 1 µg of PmE-L peptide (Lane 3) were separated on an acrylamide gel and immunoblotted with sera from sham or PmE-L-immunized mice. The red and green squares indicate PmAqp and PmE-Lm, respectively. Representative images of two experiments with similar results are shown.

AQP5E-specific Ab clones were identified

To delineate the V_H and V_L sequences of the anti-AQP5E autoantibodies, we prepared 2 sham (M1–M2) and 3 PmE-L-immunized (M3–M5) mice with varying concentrations of autoantibodies (Fig. 4A). To isolate AQP5E-specific Ab clones, we constructed phage display libraries using the draining lymph nodes from the immunized mice (Fig. 4B). After biopanning, specific binders were identified only in the M5 library, which had the highest concentration of anti-AQP5E IgG among those of the 3 immunized mice. Sequence analysis of 6 phage clones revealed that all clones used the IGHV5-6, IGHD2-3, and IGHJ2 gene segments in the V_H and IGKV14-111 and IGKJ4 gene segments in the V_L . In addition, the clones (3, 37, and 44) with a complete V_H domain had identical sequences in the CDRs of V_H and V_L , although there were mismatches in the nucleotide sequences (Fig. 5A and B, Supplementary Fig. 1). Sequencing of additional specific binder clones also revealed CDR sequences identical to those of clone 44 (data not shown).

Recombinant IgG was synthesized using the V_H and V_L encoding clone 44 and subjected to ELISA. Clone 44 recombinant IgG bound to PmE and AQP5E but not to AQP5A to confirm the specificity of the identified clones (Fig. 5C). In addition, clone 44 recombinant IgG inhibited water transport through AQP5 compared with a control clone, but this change was reversed by preincubation with the AQP5E peptide (Fig. 5D).

AQP5E-specific B cells acquired the ability to bind to AQP5E through cumulative SHM

The Ag binding sites of Abs are formed with six CDRs provided by the V_H and V_L domains, but CDR3 of the V_H domain is sufficient for most Ab specificity (29). We hypothesized that the AQP5E-specific Abs detected in the M3 and M4 mice may have substantial similarity with clone 44 in V_H CDR3 sequences. Therefore, the mismatch ratios in the V_H CDR3 sequences compared with that of clone 44 were calculated for all unique VDJ sequences in each repertoire, and clone 44-like sequences defined as those with a mismatch ratio ≤ 0.2 (i.e., similarity $\geq 80\%$) were retrieved. The 80% threshold for similarity was adopted from the literature (30). The proportion of clone 44-like sequences in M5 increased from 0.19% to 0.55% with an increase in the allowed mismatch ratio from 0 to 0.2. Clone 44-like sequences were also observed in other repertoires in the following order: M3>M4>M1>M2 (Fig. 6A). To infer the immunological status of B cells from which the VDJ sequences originated, we analyzed

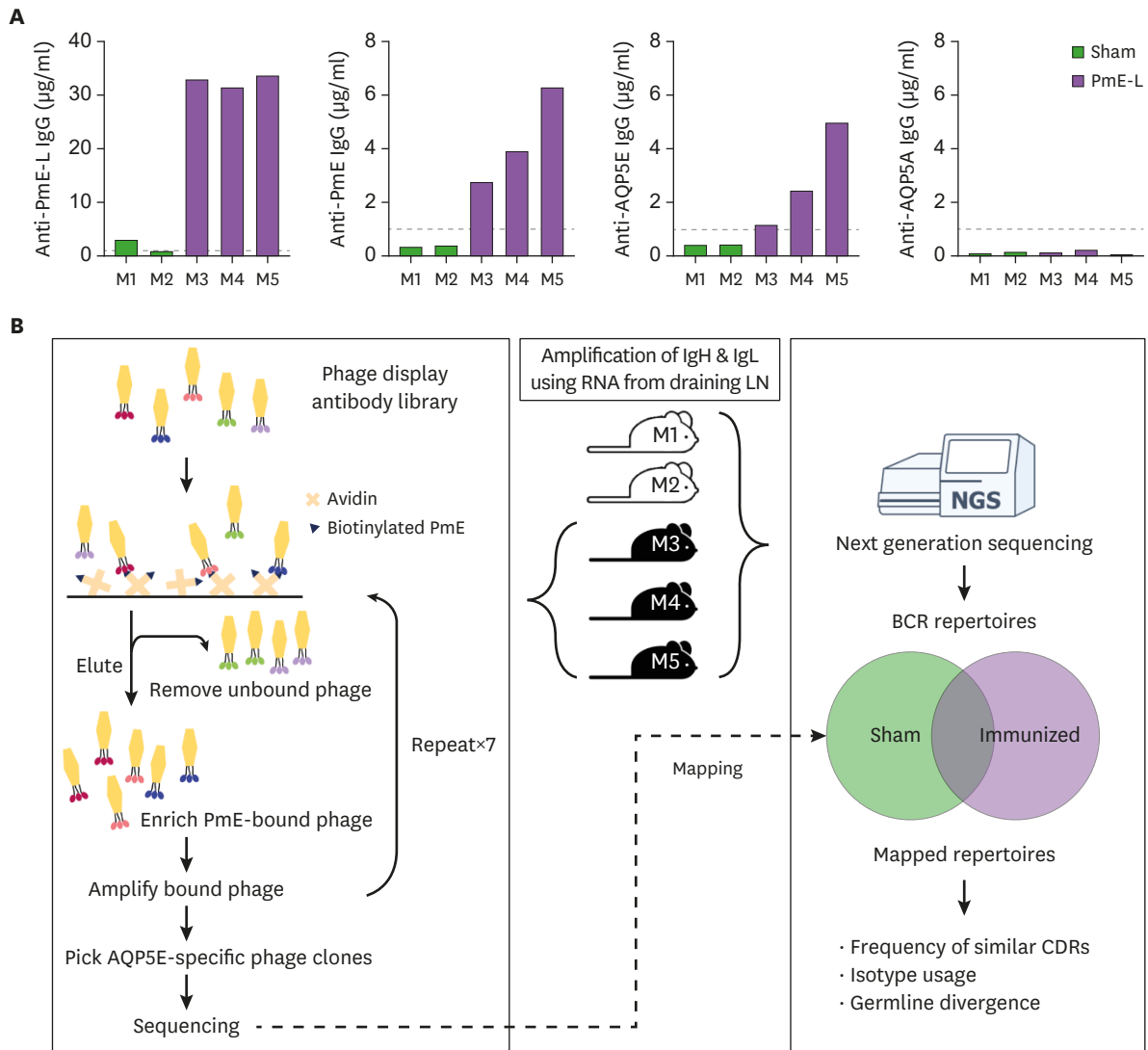


Figure 4. Experimental scheme to characterize AQP5E-specific Abs. (A) The concentrations of anti-PmE-L, anti-PmE, anti-AQP5E, and anti-AQP5A IgG in two sham (M1, M2) and three PmE-L-immunized (M3, M4, M5) mice were determined by ELISA. (B) The experimental scheme for biopanning phage display Ab libraries to identify AQP5E-specific Abs and the mapping strategy of BCR repertoires profiled by NGS.

the isotype compositions of the clone 44-like sequences. All sequences from the M1 and M2 sham mice were IgM isotypes, which are known as the naïve form of Abs, while the sequences from the PmE-L-immunized mice were predominantly IgG1 isotypes (**Fig. 6B**). When the same analysis was applied only to VDJ sequences from the IGHV5-6 gene, clone 44-like sequences were found only in M5, which were also dominated by the IgG1 isotype (**Fig. 6C and D**).

We also analyzed the frequencies of IGHV5-6 gene usage in each repertoire by isotype. According to the literature, the frequency of IGHV5-6 usage in the IgM-associated VDJ rearrangements of C57BL/6 splenocytes is 0.38% (31). The frequency of IGHV5-6 usage in the IgM-associated sequences was particularly low (0.05%) in M5, provably due to activation and isotype switching of some of the IgM clones. Although the frequency of the IGHV5-6-used IgG1-associated sequences was as high as 1.2% in M5, it was even higher in M2, one of the sham mice, indicating that the abundance of IGHV5-6-used sequences does not necessarily reflect the expansion of AQP5E-specific B cells (**Fig. 6E**).

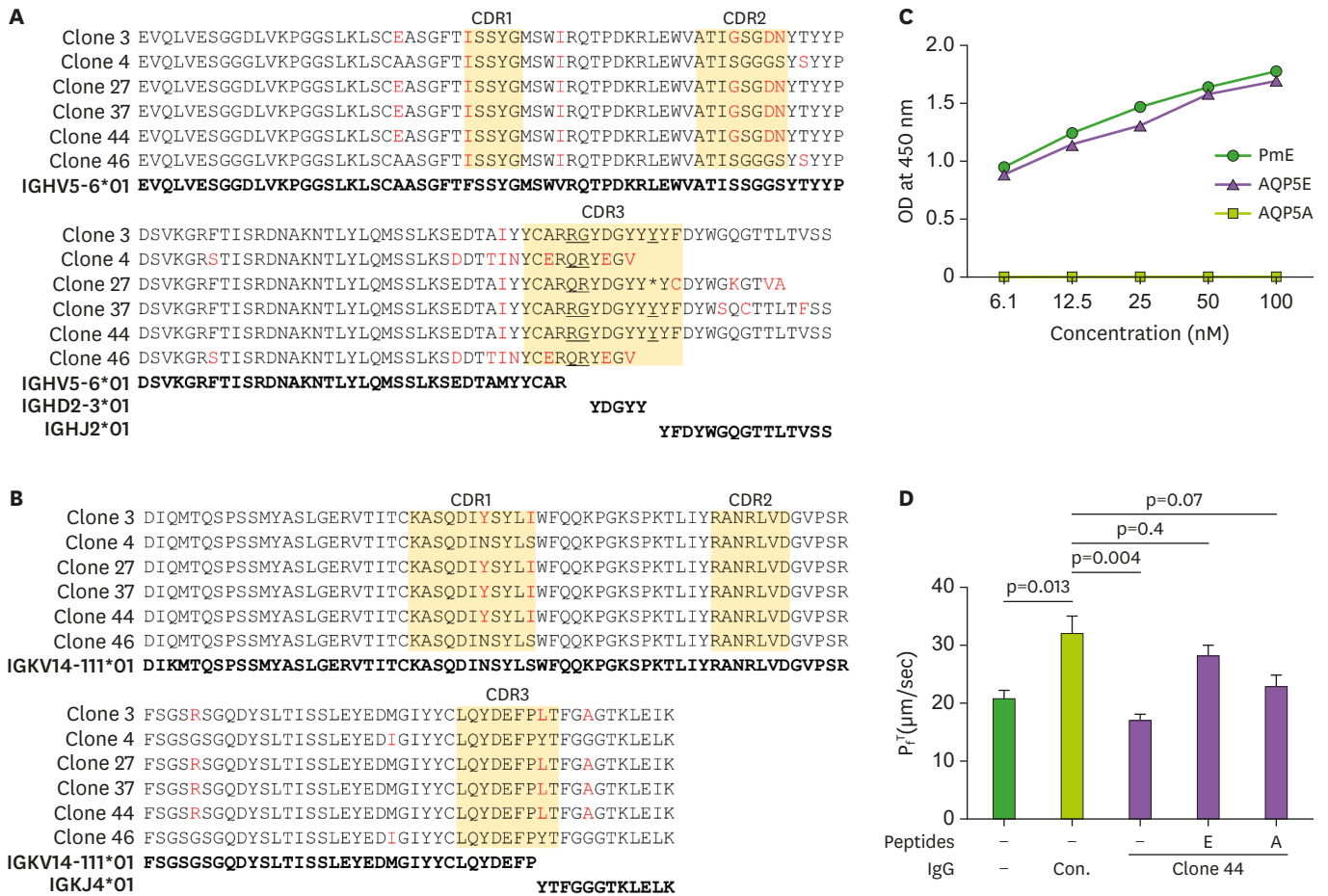


Figure 5. AQP5E-specific Ab clones were identified. Six AQP5E-specific phage clones were identified through biopanning phage Ab libraries. The amino acid sequences of the V_H (A) and V_L (B) were compared with those of germline gene segments, and three CDRs were annotated. (C) Recombinant IgG produced using the variable genes of clone 44 was subjected to ELISA to confirm specific binding to PmE and AQP5E. (D) The effects of clone 44 recombinant IgG and neutralizing peptides on P_i in MDCK-AQP5 cells were determined 20 min after osmotic challenge and compared with that of control recombinant IgG by t-test. Each column presents the mean±SEM of 2 experiments performed in triplicate.

For determination of whether B cells experienced affinity maturation pressure by immunization, the divergence of the IGHV5-6-used sequences from the V gene was computed and compared between the sham and PmE-L-immunized groups by isotypes. Sequences associated with IgG1, IgG2b, IgG2c, and IgM had significantly more SHM in the PmE-L-immunized group than in the sham group (Fig. 6F). Scatter plots of the divergence of the IGHV5-6-used sequences against similarity to clone 44 in V_H CDR3 revealed that the limited SHM observed in the sham group did not increase the similarity compared with those without SHM. In contrast, like clone 44, which had a divergence of 0.034, most clone 44-like sequences (similarity $\geq 80\%$) in the PmE-L group had a divergence >0.02 . In addition, the similarity to clone 44 had a positive correlation with divergence, suggesting that the AQP5E-specific B cells acquired the ability to bind to AQP5E through cumulative SHM.

DISCUSSION

In this study, we characterized the Ag specificity and variable gene sequences of AQP5E-binding Abs along with salivary gland phenotypes in an anti-AQP5 autoantibody-producing mouse model.

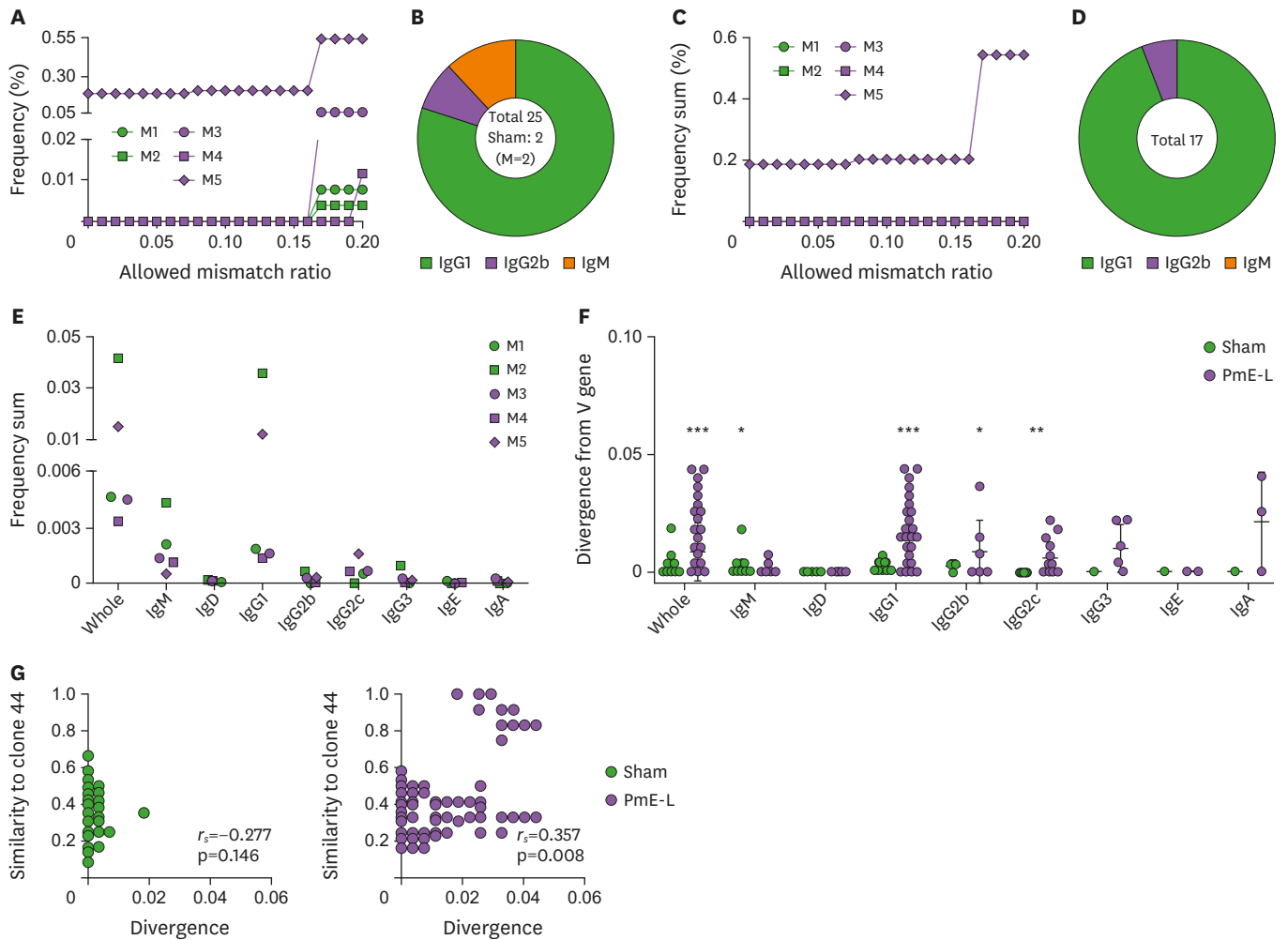


Figure 6. AQP5E-specific B cells acquired affinity to AQP5E through the accumulation of somatic hypermutations. BCR repertoires of two sham and three PmE-L-immunized mice were profiled by NGS. (A) The V_H CDR3 in each unique VDJ sequence was compared with that of clone 44. After clone 44-like sequences defined as those with mismatch ratios ≤ 0.2 (i.e., similarity $\geq 80\%$) were retrieved, the sum of the clonal frequencies in each repertoire was plotted against the allowed mismatch ratios. (B) Distribution of the isotypes among the clone 44-like sequences presented in A. (C) Among the clone 44-like sequences presented in A, only the IGHV5-6 gene-used sequences were plotted. (D) Distribution of isotypes among the clone 44-like sequences presented in C. (E) Frequencies of the IGHV5-6 gene-used sequences in each repertoire by isotype. (F) The divergences of the IGHV5-6 gene-used sequences from the V gene were compared between the sham and PmE-L-immunized mice by isotype. (G) Scatter plots for the divergence of the IGHV5-6 gene-used sequences from the V gene over similarity to clone 44 V_H CDR3. A correlation between the two variables was determined by Spearman's rank correlation coefficient.

* $p < 0.05$; ** $p < 0.01$; *** $p < 0.001$ by Mann-Whitney U test.

Repeated immunization with the PmAqp-derived peptide PmE-L efficiently induced anti-AQP5E autoantibodies through molecular mimicry. There was a strong positive correlation between the levels of anti-PmE IgG and those of anti-AQP5E IgG (Fig. 2C). The sera containing the anti-AQP5E IgG not only stained mouse Aqp5 expressed in the submandibular glands but also detected PmAqp and the immunizing peptide by immunoblotting (Fig. 3A and B). Furthermore, recombinant clone 44 IgG, which was produced using the variable genes encoding the AQP5E-specific phage clone 44, bound to both PmE and AQP5E. All these findings indicate that the Abs produced against PmE are cross-reactive with AQP5E. This cross-reactivity is not surprising since there is only one amino acid difference between PmE and AQP5E, and the predicted structure of PmE-L mimics the structure of AQP5E located in mouse Aqp5 (Fig. 1).

Characterization of AQP5E-specific autoantibodies selected from the screening of phage display Ab libraries and mapping of the BCR repertoires revealed that the AQP5E-specific B cells acquired the ability to bind to the Ag through cumulative SHM. Interestingly, all AQP5E-specific clones, including clone 44, picked in the phage Ab library of M5 used the IGHV5-6 gene segment, and the divergences of the IGHV5-6-used sequences were significantly increased in the PmE-L-immunized repertoires compared with the sham repertoires, particularly in the IgG-associated sequences (**Figs. 5A** and **6F**). Furthermore, most clone 44-like sequences identified in the PmE-L-immunized repertoires had divergence >0.02 , while the IGHV5-6-used sequences in the sham repertoires had divergence <0.02 (**Fig. 6G**). This finding indicates that clone 44 and other AQP5E-specific clones gained the ability to bind to AQP5E through SHM. The PmE-L peptide used in immunization must have driven SHM and selection as a foreign Ag.

Importantly, the presence of anti-AQP5E autoantibodies was associated with a low salivary flow rate in mice (**Fig. 2C**), suggesting the role of anti-AQP5 autoantibodies in the dryness of SS patients. Inhibition of water permeability through AQP5 expressed in MDCK cells by recombinant clone 44 IgG (**Fig. 5D**) supports this notion. However, there was a broad variation in salivary flow rates among the mice with the same levels of anti-AQP5E IgG. The concentrations of Abs determined by ELISAs do not reflect affinity to Ags, and the ability of each clone of the polyclonal anti-AQP5E autoantibodies to interfere with AQP5 function must vary. In addition, seven mice positive for anti-M3R autoantibodies, which also interfere with the salivary secretion process, were distributed in all 3 groups. These factors may account for the variable associations of anti-AQP5 autoantibodies with low salivary flow rates in SS patients (5,8).

Despite the reduced salivary flow rate, no histologic abnormality was observed in the salivary glands of the mice with anti-AQP5E autoantibodies. Similarly, no immune cell infiltration was reported in curdlan-injected SKG mice despite increased IgG deposition in the salivary glands and reduced salivary flow rates (32). The authors attributed this finding to the fact that IgG1 was the major isotype of autoantibody produced and that murine IgG1 is ineffective in complement and FcR activation. In IgG4-related diseases in humans, however, the deposition of IgG4, the human version of murine IgG1, is associated with sialadenitis (33). Induction of focal lymphocytic sialadenitis in C57BL/6 mice by repeated immunization with salivary gland proteins emulsified in Freund's complete adjuvant has been shown; this condition was aggravated at 30 weeks after the first immunization compared with that at week 5 and depended on Th17 cells (34). When we boosted mice on days 10, 24, and 64 and then examined the salivary glands of the mice on day 110 in our other experiments, we still found no sialadenitis, although the anti-AQP5E autoantibodies were detected (data not shown). The results of three different models suggest that salivary gland-targeting autoantibodies alone do not necessarily lead to focal lymphocytic sialadenitis. Infection of the salivary glands with bacteria observed in SS patients may also contribute to immune cell infiltration (15).

Repeated immunization with Pm lysates induced anti-AQP5E autoantibodies in only 11% of the immunized mice, although the concentrations of total IgG were higher than those in the PmE-L group. The reason for this inefficient induction of anti-AQP5E autoantibody production by Pm is mainly due to the paucity of Ag. The amount of protein in 1×10^7 Pm cells used for immunization was approximately 80 μg . According to the immunoblotting results (**Fig. 2G**), the molar amount of PmAqp present in the 80 μg Pm lysates was estimated to be lower than 1 μg PmE-L peptide. In SS patients, the infection of salivary glands with Pm (15) may contribute to the production of anti-AQP5 autoantibodies not only through molecular mimicry but also via bystander activation of APCs.

In this model, Pm lysate, which was used for priming, and IFA can provide bystander activation of APCs. Anti-M3R autoantibodies detected in several mice may be due to bystander activation because one of the anti-M3R Ab-positive mice was in the sham group, and M3R is ubiquitously expressed, including in muscle, adipose, and lymphoid tissues (35). However, Aqp5 is not expressed at the injection site or lymph nodes (35). Hence, bystander activation of APCs could not drive the production of anti-AQP5E autoantibodies. We previously reported no production of Abs against AQP5A, another epitope of anti-AQP5 autoantibodies, by immunization with PmE-L (17), which supports no role for bystander activation of APCs in the anti-AQP5E autoantibody induction in this model.

Aquaporins are transmembrane proteins and do not maintain proper structures in soluble forms. Therefore, instead of using recombinant PmAqp, we designed a peptide that contains both a T cell epitope and a conserved functional B cell epitope for immunization (17). Recently, Tsymala et al. (36) reported a rat model that produces AQP4-reactive Abs by immunization with AQP4 mimotopes. These researchers screened a phage display peptide library to search for AQP4 mimotopes recognized by pathogenic AQP4-specific Abs from patients with neuromyelitis optica spectrum disorders (36). Our approach to identify a mimotope in a homologous bacterial protein was proven to be effective.

The multiple bands detected in the immunoblotting of Pm lysates with the PmE-L immunized sera may be attributed to cross-reaction of anti-PmE-L IgG to other proteins in Pm lysates. A BLAST search against Pm proteins using PmE-L as a query revealed several additional proteins that matched some PmE-L sequences: aquaporin family protein (25.9 kDa), methyltransferase (26.4 kDa), HAD family hydrolase (30.22 kDa), hypothetical protein HMPREF0659_A7004 (32.73 kDa), YitT family protein (33.84 kDa), hypothetical protein HMPREF0659_A7160 (34.25 kDa), membrane protein (34.49 kDa), 3-deoxy-D-manno-octulosonic-acid transferase (46.71 kDa), serine acetyltransferase (60.74 kDa), and TonB-dependent receptor (93.22 kDa).

In conclusion, we developed a mouse model that produces anti-AQP5 autoantibodies by molecular mimicry. Although this model is not suitable as an SS model due to the lack of focal lymphocytic sialadenitis and anti-SSA autoantibodies, it will be useful to investigate the role of anti-AQP5 autoantibodies in glandular dysfunction in SS. Furthermore, the tools to easily detect autoantibodies and autoantigen-specific B cells allow this model to be used to test new therapeutics targeting autoantibody production.

ACKNOWLEDGEMENTS

This study was supported by the National Research Foundation of Korea (Daejun, Korea) through the grants 2018R1A5A2024418 and 2020R1A2C2007038 awarded to Youngnim Choi.

SUPPLEMENTARY MATERIAL

Supplementary Figure 1

The nucleotide sequences of the V_H and V_L of 3 AQP5E-specific phage clones.

[Click here to view](#)

REFERENCES

1. Thorne I, Sutcliffe N. Sjögren's syndrome. *Br J Hosp Med (Lond)* 2017;78:438-442.
[PUBMED](#) | [CROSSREF](#)
2. Christodoulou MI, Kapsogeorgou EK, Moutsopoulos HM. Characteristics of the minor salivary gland infiltrates in Sjögren's syndrome. *J Autoimmun* 2010;34:400-407.
[PUBMED](#) | [CROSSREF](#)
3. Routsias JG, Tzioufas AG. Sjögren's syndrome--study of autoantigens and autoantibodies. *Clin Rev Allergy Immunol* 2007;32:238-251.
[PUBMED](#) | [CROSSREF](#)
4. Scofield RH, Fayyaz A, Kurien BT, Koelsch KA. Prognostic value of Sjögren's syndrome autoantibodies. *J Lab Precip Med* 2018;3:92.
[PUBMED](#) | [CROSSREF](#)
5. Alam J, Koh JH, Kim N, Kwok SK, Park SH, Song YW, Park K, Choi Y. Detection of autoantibodies against aquaporin-5 in the sera of patients with primary Sjögren's syndrome. *Immunol Res* 2016;64:848-856.
[PUBMED](#) | [CROSSREF](#)
6. Matsuzaki T, Susa T, Shimizu K, Sawai N, Suzuki T, Aoki T, Yokoo S, Takata K. Function of the membrane water channel aquaporin-5 in the salivary gland. *Acta Histochem Cytochem* 2012;45:251-259.
[PUBMED](#) | [CROSSREF](#)
7. Alam J, Koh JH, Kwok SK, Park SH, Park K, Choi Y. Functional epitopes for anti-aquaporin 5 antibodies in Sjögren syndrome. *J Dent Res* 2017;96:1414-1421.
[PUBMED](#) | [CROSSREF](#)
8. Jeon S, Lee J, Park SH, Kim HD, Choi Y. Associations of anti-aquaporin 5 autoantibodies with serologic and histopathological features of Sjögren's syndrome. *J Clin Med* 2019;8:1863.
[PUBMED](#) | [CROSSREF](#)
9. Nemazee D. Mechanisms of central tolerance for B cells. *Nat Rev Immunol* 2017;17:281-294.
[PUBMED](#) | [CROSSREF](#)
10. Abramson J, Husebye ES. Autoimmune regulator and self-tolerance - molecular and clinical aspects. *Immunol Rev* 2016;271:127-140.
[PUBMED](#) | [CROSSREF](#)
11. Alam J, Kim YC, Choi Y. Potential role of bacterial infection in autoimmune diseases: a new aspect of molecular mimicry. *Immune Netw* 2014;14:7-13.
[PUBMED](#) | [CROSSREF](#)
12. Igoe A, Scofield RH. Autoimmunity and infection in Sjögren's syndrome. *Curr Opin Rheumatol* 2013;25:480-487.
[PUBMED](#) | [CROSSREF](#)
13. Bartoloni E, Alunno A, Gerli R. The dark side of Sjögren's syndrome: the possible pathogenic role of infections. *Curr Opin Rheumatol* 2019;31:505-511.
[PUBMED](#) | [CROSSREF](#)
14. Maślińska M. The role of Epstein-Barr virus infection in primary Sjögren's syndrome. *Curr Opin Rheumatol* 2019;31:475-483.
[PUBMED](#) | [CROSSREF](#)
15. Alam J, Lee A, Lee J, Kwon DI, Park HK, Park JH, Jeon S, Baek K, Lee J, Park SH, et al. Dysbiotic oral microbiota and infected salivary glands in Sjögren's syndrome. *PLoS One* 2020;15:e0230667.
[PUBMED](#) | [CROSSREF](#)
16. Alam J, Choi YS, Koh JH, Kwok SK, Park SH, Song YW, Park K, Choi Y. Detection of autoantibodies against aquaporin-1 in the sera of patients with primary Sjögren's syndrome. *Immune Netw* 2017;17:103-109.
[PUBMED](#) | [CROSSREF](#)
17. Lee A, Choi Y. Induction of anti-aquaporin 5 autoantibodies by molecular mimicry in mice. *Int J Oral Biol* 2020;45:211-217.
[CROSSREF](#)
18. Kim N, Shin Y, Choi S, Namkoong E, Kim M, Lee J, Song Y, Park K. Effect of antimuscarinic autoantibodies in primary Sjögren's syndrome. *J Dent Res* 2015;94:722-728.
[PUBMED](#) | [CROSSREF](#)
19. Barbas CF 3rd, Burton DR, Scott JK, Silverman GJ. Phage display. In: *A Laboratory Manual*. Suffolk County, NY: Cold Spring Harbor Laboratory Press; 2001.
20. Yoo DK, Lee SR, Jung Y, Han H, Lee HK, Han J, Kim S, Chae J, Ryu T, Chung J. Machine learning-guided prediction of antigen-reactive in silico clonotypes based on changes in clonal abundance through bio-panning. *Biomolecules* 2020;10:421.
[PUBMED](#) | [CROSSREF](#)

21. Smith T, Heger A, Sudbery I. UMI-tools: modeling sequencing errors in Unique Molecular Identifiers to improve quantification accuracy. *Genome Res* 2017;27:491-499.
[PUBMED](#) | [CROSSREF](#)
22. Zhang J, Kobert K, Flouri T, Stamatakis A. PEAR: a fast and accurate Illumina Paired-End reAd mergeR. *Bioinformatics* 2014;30:614-620.
[PUBMED](#) | [CROSSREF](#)
23. Kim SI, Noh J, Kim S, Choi Y, Yoo DK, Lee Y, Lee H, Jung J, Kang CK, Song KH, et al. Stereotypic neutralizing V_H antibodies against SARS-CoV-2 spike protein receptor binding domain in patients with COVID-19 and healthy individuals. *Sci Transl Med* 2021;13:eabd6990.
[PUBMED](#) | [CROSSREF](#)
24. Ye J, Ma N, Madden TL, Ostell JM. IgBLAST: an immunoglobulin variable domain sequence analysis tool. *Nucleic Acids Res* 2013;41:W34-W40.
[PUBMED](#) | [CROSSREF](#)
25. Lefranc MP, Lefranc G. Immunoglobulins or antibodies: IMGT® bridging genes, structures and functions. *Biomedicines* 2020;8:319.
[PUBMED](#) | [CROSSREF](#)
26. Jin J, Park G, Park JB, Kim S, Kim H, Chung J. An anti-EGFR × cotinine bispecific antibody complexed with cotinine-conjugated duocarmycin inhibits growth of EGFR-positive cancer cells with KRAS mutations. *Exp Mol Med* 2018;50:1-14.
[PUBMED](#) | [CROSSREF](#)
27. Kim SI, Kim S, Shim JM, Lee HJ, Chang SY, Park S, Min JY, Park WB, Oh MD, Kim S, et al. Neutralization of Zika virus by E protein domain III-Specific human monoclonal antibody. *Biochem Biophys Res Commun* 2021;545:33-39.
[PUBMED](#) | [CROSSREF](#)
28. Levin MH, Sullivan S, Nielson D, Yang B, Finkbeiner WE, Verkman AS. Hypertonic saline therapy in cystic fibrosis: Evidence against the proposed mechanism involving aquaporins. *J Biol Chem* 2006;281:25803-25812.
[PUBMED](#) | [CROSSREF](#)
29. Xu JL, Davis MM. Diversity in the CDR3 region of V_H is sufficient for most antibody specificities. *Immunity* 2000;13:37-45.
[PUBMED](#) | [CROSSREF](#)
30. Briney B, Inderbitzin A, Joyce C, Burton DR. Commonality despite exceptional diversity in the baseline human antibody repertoire. *Nature* 2019;566:393-397.
[PUBMED](#) | [CROSSREF](#)
31. Collins AM, Wang Y, Roskin KM, Marquis CP, Jackson KJ. The mouse antibody heavy chain repertoire is germline-focused and highly variable between inbred strains. *Philos Trans R Soc Lond B Biol Sci* 2015;370:20140236.
[PUBMED](#) | [CROSSREF](#)
32. Choi SS, Jang E, Jang K, Jung SJ, Hwang KG, Youn J. Autoantibody-mediated dysfunction of salivary glands leads to xerostomia in SKG mice. *Immune Netw* 2019;19:e44.
[PUBMED](#) | [CROSSREF](#)
33. Deshpande V. IgG4 related disease of the head and neck. *Head Neck Pathol* 2015;9:24-31.
[PUBMED](#) | [CROSSREF](#)
34. Lin X, Rui K, Deng J, Tian J, Wang X, Wang S, Ko KH, Jiao Z, Chan VS, Lau CS, et al. Th17 cells play a critical role in the development of experimental Sjögren's syndrome. *Ann Rheum Dis* 2015;74:1302-1310.
[PUBMED](#) | [CROSSREF](#)
35. Uhlén M, Fagerberg L, Hallström BM, Lindskog C, Oksvold P, Mardinoglu A, Sivertsson Å, Kampf C, Sjöstedt E, Asplund A, et al. Proteomics. Tissue-based map of the human proteome. *Science* 2015;347:1260419.
[PUBMED](#) | [CROSSREF](#)
36. Tsymala I, Nigritinou M, Zeka B, Schulz R, Niederschick F, Matković M, Bauer JJ, Szalay M, Schanda K, Lerch M, et al. Induction of aquaporin 4-reactive antibodies in Lewis rats immunized with aquaporin 4 mimotopes. *Acta Neuropathol Commun* 2020;8:49.
[PUBMED](#) | [CROSSREF](#)